

## Electronic Supplementary Information

### Chloroformamidine hydrochloride as a molecular linker towards efficient and stable perovskite solar cells

Hui Li,<sup>ab</sup> Ping Fu,<sup>a</sup> Ruixue Lu,<sup>ac</sup> Junxun Guo,<sup>ad</sup> Xin Guo,<sup>a</sup> Rengui Li<sup>a</sup> and Can Li<sup>\*ab</sup>

<sup>a</sup> State Key Laboratory of Catalysis, Dalian National Laboratory for Clean Energy, Dalian Institute of Chemical Physics, Chinese Academy of Sciences, Zhongshan Road 457, Dalian, 116023 (China).

<sup>b</sup> University of Chinese Academy of Sciences, Beijing, 100049 (China).

<sup>c</sup> Department of Chemistry, iChEM (Collaborative Innovation Center of Chemistry for Energy Materials), Fudan University, Shanghai, 200438 (China).

<sup>d</sup> School of Chemistry and Materials Science, University of Science and Technology of China, Hefei, 230026 (China).

\* Corresponding author

E-mail: canli@dicp.ac.cn

## Experimental Procedures

### Materials

All chemicals used in this work are commercially available and were used without additional purification steps. The SnO<sub>2</sub> aqueous colloid (15.0 wt%) was obtained from Alfa Aesar (tin(IV) oxide). *N,N*-dimethylformamide (DMF) and dimethyl sulfoxide (DMSO) were purchased from Sigma-Aldrich. Isopropanol (IPA) was purchased from Aladdin. Lead iodide (PbI<sub>2</sub>) (99.99%), formamidinium iodide (FAI) (99.5%), methylammonium bromide (MABr) (99.9%), methylammonium chloride (MACl) (99.5%) and 2,2',7,7'-tetrakis(*N,N*-di-*p*-methoxyphenylamine)-9,9'-spirobifluorene (Spiro-OMeTAD) (99.5%) were purchased from Advanced Election Technology CO., Ltd. Bis(trifluoromethane)sulfonimide lithium salt (Li-TFSI) was purchased from Sigma-Aldrich. FK209 (Co(III)TFSI) and 4-*tert*-Butylpyridine (*t*BP) were purchased from Xi'an Polymer Light Technology Corp, China. Chloroformamidine hydrochloride (CFA) (98.0%) was obtained from Aladdin.

### Device fabrication

ITO substrates were cleaned by sequentially washing with ethanol, IPA and ethanol in ultrasonic bath for 30 min each, then dried by flowing nitrogen and treated with UV-ozone for 30 min before use. The SnO<sub>2</sub> aqueous colloidal (15.0 wt%) was diluted using deionized water to the concentration of 3.0 wt%. Then CFA (0.2–1.0 mg mL<sup>-1</sup>) was added into the SnO<sub>2</sub> aqueous colloidal (3.0 wt%) to obtain CFA@SnO<sub>2</sub> precursor solutions. These solutions were stirred at room temperature for 30 minutes. The SnO<sub>2</sub> and CFA@SnO<sub>2</sub> layers were fabricated by spin-coating SnO<sub>2</sub> or CFA@SnO<sub>2</sub> precursor solutions on ITO substrates at 4000 r.p.m. for 30 s, and then annealed for 30 min at 150 °C in ambient air. Once cooled to room temperature, the samples were treated with UV-ozone for 25 min before making perovskite films.

The FAPbI<sub>3</sub>-based perovskite films were deposited on different ETLs using two-step spin coating method.<sup>1</sup> First, the precursor PbI<sub>2</sub> (691.5 mg, 1.5 mol L<sup>-1</sup>) dissolved in DMF/DMSO (v/v 9/1) solution was spin-coated onto the SnO<sub>2</sub> or CFA@SnO<sub>2</sub> substrates at 1500 r.p.m. for 30 s, and then annealed at 70 °C for 1 min. Second, after the PbI<sub>2</sub> film cooled down to room temperature, 50 μL of the organic mixture solution

of FAI: MABr: MACl (60 mg : 6 mg : 9 mg in 1 mL IPA) was spin-coated onto the  $\text{PbI}_2$  film at 1700 r.p.m for 30 s. When the resulting films turned from orange to dark brown in glove box, they were taken out from the glove box and thermally annealed at 150 °C for 15 min in ambient air (30%–40% humidity). It has reported that humidity is beneficial in obtaining high-quality perovskite films.<sup>2</sup> Then films were transferred into a  $\text{N}_2$ -filled glovebox.

Then, the Spiro-OMeTAD solution, which consisted of 72.3 mg Spiro-OMeTAD, 17.5  $\mu\text{L}$  Li-TFSI stock solution (520 mg Li-TFSI in 1 ml acetonitrile), 29  $\mu\text{L}$  FK209 stock solution (300 mg FK209 in 1 ml acetonitrile), 29  $\mu\text{L}$  tBP and 1 mL chlorobenzene, was spin-coated on top of the perovskite layer at 3000 r.p.m for 30 s as the hole transport layer. These samples were retained in a desiccator overnight. Finally, 100 nm Au film was deposited via thermal evaporation as a counter electrode. The device area of 0.04  $\text{cm}^2$  and 0.10  $\text{cm}^2$  were determined by a metal mask.

### **Characterization**

Photocurrent density–voltage (J-V) curves were measured using a solar simulator (SS-F5-3A, Enlitech) along with AM 1.5G spectra whose intensity was calibrated by certified standard silicon solar cell (SRC-2020, Enlitech) at 100  $\text{mW cm}^{-2}$ , and a Keithley 2400 source meter. J-V curves were measured from -0.1 V to 1.2 V (forward scan, FS) or from 1.2 V to -0.1 V (reverse scan, RS) with a scan rate of 20  $\text{mV s}^{-1}$ .

X-ray diffraction (XRD) patterns were acquired with a Rigaku SmartLab diffractometer using Cu  $\text{K}\alpha$  radiation provided applied current and voltage values of 200 mA and 40 kV, respectively. The scan rate of 20 °/min was applied to record the XRD patterns in the range of 5–60° (2 theta). Scanning electron microscopy (SEM) was performed on a JSM-7800F microscope (JEOL) with an accelerating voltage of 3 kV. UV-visible (UV-vis) absorption spectra were recorded on a UV-vis spectrophotometer (JASCO V-650). The Attenuated total reflectance-Fourier transform infrared (ATR-FTIR) spectra were recorded with a Nicolet iS50 infrared Fourier transform microscope by Thermo-Fisher Scientific. A Fluorescence spectrophotometer (QM400, PTI) with an excitation wavelength of 520 nm was used to collect steady-state photoluminescence (PL) spectra. The time-resolved PL (TRPL)

spectra were recorded on a FLS920 fluorescence spectrometer (Edinburgh Instruments) in air at room temperature. A picosecond pulsed diode laser (406.8 nm) was used as the excitation source.

X-ray photoelectron spectroscopy (XPS) measurements were performed on a Thermo-Fisher ESCALAB 250Xi system with a monochromatized Al K $\alpha$  under the pressure of  $4.0 \times 10^{-9}$  mbar and all the binding energies were calibrated by C 1s (284.8 eV) as a reference. Ultraviolet photoelectron spectroscopy (UPS) was performed on a photoelectron spectrometer (Thermo-Fisher ESCALAB XI+). The contact angle was measured using a DSA100 optical contact-measuring system (KRUSS).

### **Electron mobility of SnO<sub>2</sub> and CFA@SnO<sub>2</sub> film**

The space charge-limited current (SCLC) method<sup>3</sup> was employed to measure the electron mobility of SnO<sub>2</sub> film and CFA@SnO<sub>2</sub> film. Specifically, the electron-only device was designed and fabricated using ITO/ETL/Au structure, as shown in the inset in Fig. 1e. The dark J-V curves of the devices were performed on a Keithley 2400 source meter. The electron mobility ( $\mu_e$ ) is extracted by fitting the J-V curves using the Mott-Gurney law (1):

$$\mu_e = \frac{8JL^3}{9\varepsilon_0\varepsilon_r(V_{app} - V_r - V_{bi})^2} \quad (1)$$

where  $\mu_e$  is the electron mobility, J is the current density, L is the thickness of SnO<sub>2</sub> film,  $\varepsilon_0$  is the vacuum permittivity,  $\varepsilon_r$  is the relative dielectric permittivity of SnO<sub>2</sub> ( $\varepsilon_r = 9.9$ ),  $V_{app}$  is the applied voltage,  $V_r$  is the voltage loss due to constant resistance and series resistance across the electrodes, and  $V_{bi}$  is the built-in voltage owing to the different work function between the anode and cathode.

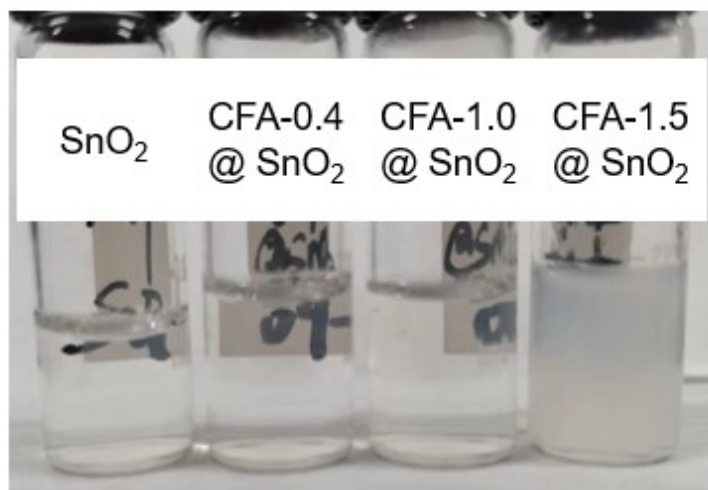


**Fig. S1.** Photographs of the SnO<sub>2</sub> (3.0 wt%) colloidal solution with different CFA amounts (0, 0.4, 1.0, 1.5 mg mL<sup>-1</sup>, respectively).

The surface of SnO<sub>2</sub> nanoparticles is negatively charged in colloid solution. In addition, KOH is added as a stabilizer in commercial SnO<sub>2</sub> colloid solution to well-disperse the ultra-small nanoparticles.<sup>4, 5</sup> We investigated the effect of CFA concentration with the acidic property on SnO<sub>2</sub> colloid solution. As the result, the mixed solution remains clear and transparent after introducing 0.4 mg mL<sup>-1</sup> and 1.0 mg mL<sup>-1</sup> CFA, but it becomes milky white jelly by introducing 1.5 mg mL<sup>-1</sup> CFA.

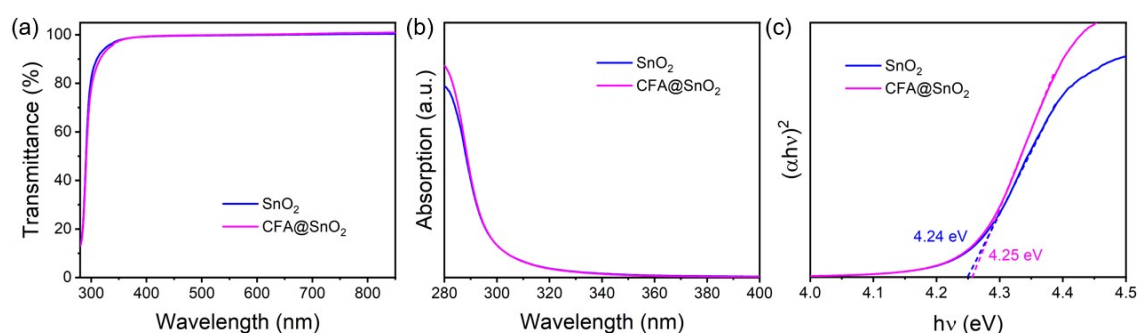


**Fig. S2.** (a) Transmittance spectra. (b) UV-vis absorption spectra. (c) Tauc plot derived from UV-vis absorption spectra of SnO<sub>2</sub> and CFA@SnO<sub>2</sub> films deposited on glass, respectively.

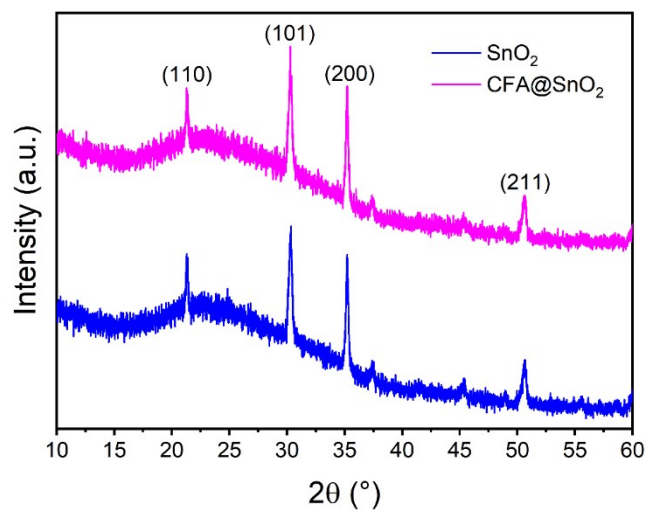


**Fig. S3.** XRD patterns of SnO<sub>2</sub> and CFA@SnO<sub>2</sub> films, respectively.

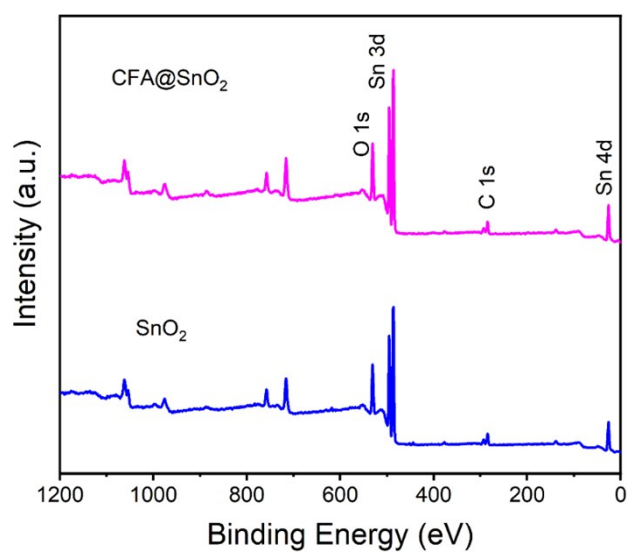


**Fig. S4.** XPS spectra of SnO<sub>2</sub> and CFA@SnO<sub>2</sub> films, respectively.

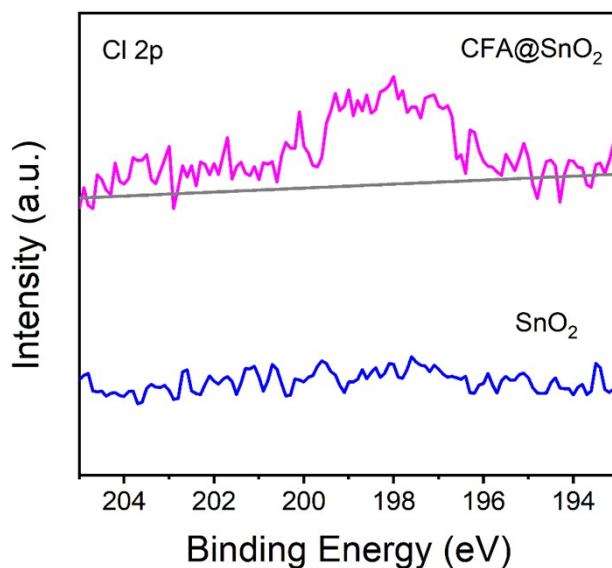


**Fig. S5.** XPS spectra of the Cl 2p orbital of SnO<sub>2</sub> and CFA@SnO<sub>2</sub> films, respectively.

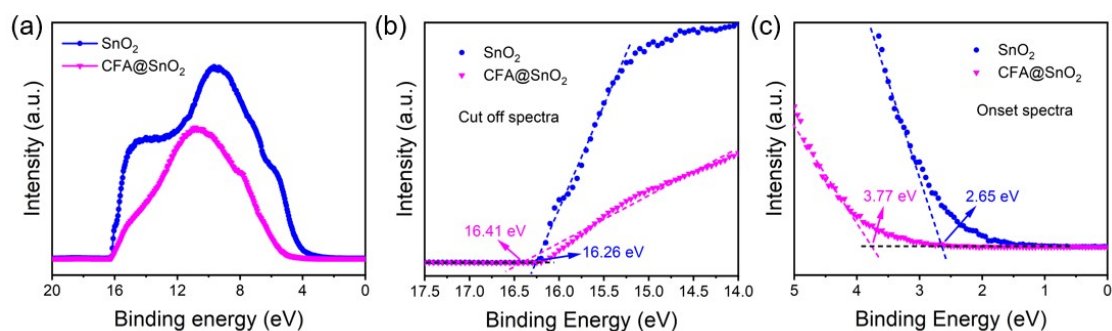


**Fig. S6.** (a) UPS spectra. (b) The electron cut off region and (c) the valence band region of the UPS spectra for SnO<sub>2</sub> and CFA@SnO<sub>2</sub> films, respectively.

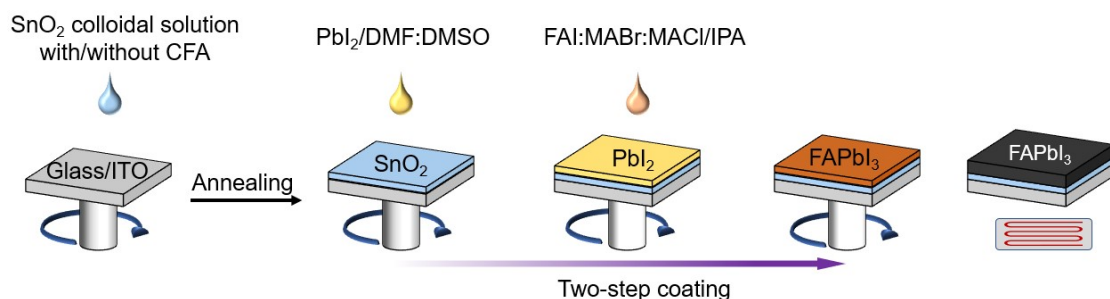


**Fig. S7.** Schematic diagram of the manufacturing process for SnO<sub>2</sub> films and perovskite films.

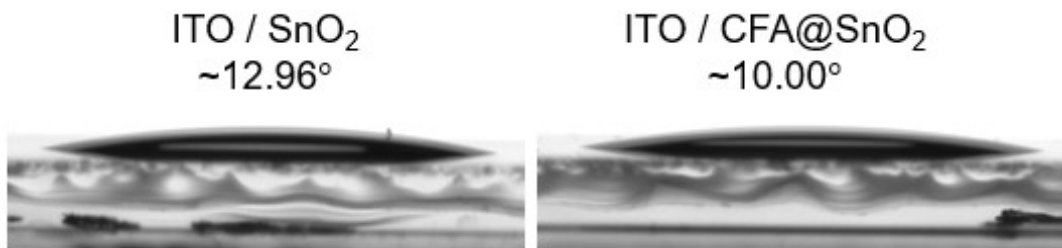


**Fig. S8.** Water contact angles measured on SnO<sub>2</sub> and CFA@SnO<sub>2</sub> films, respectively.

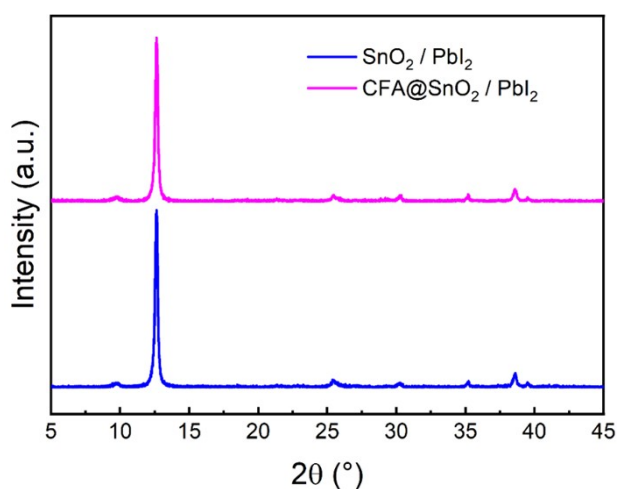


**Fig. S9.** XRD patterns of Pbl<sub>2</sub> films deposited on SnO<sub>2</sub> and CFA@SnO<sub>2</sub> substrates, respectively.

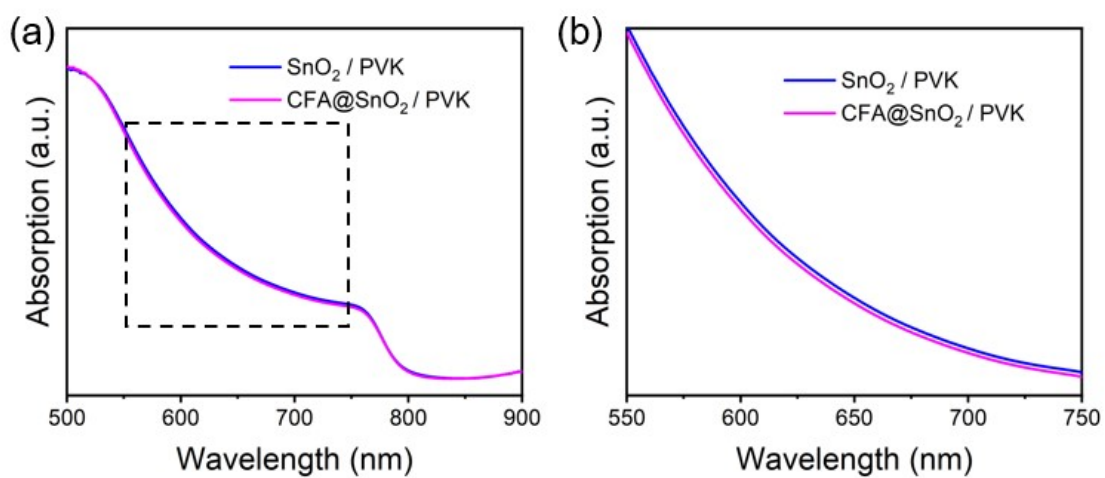


**Fig. S10.** (a) UV-vis absorption spectra. (b) The enlarged part of the dotted box part in Figure (a).

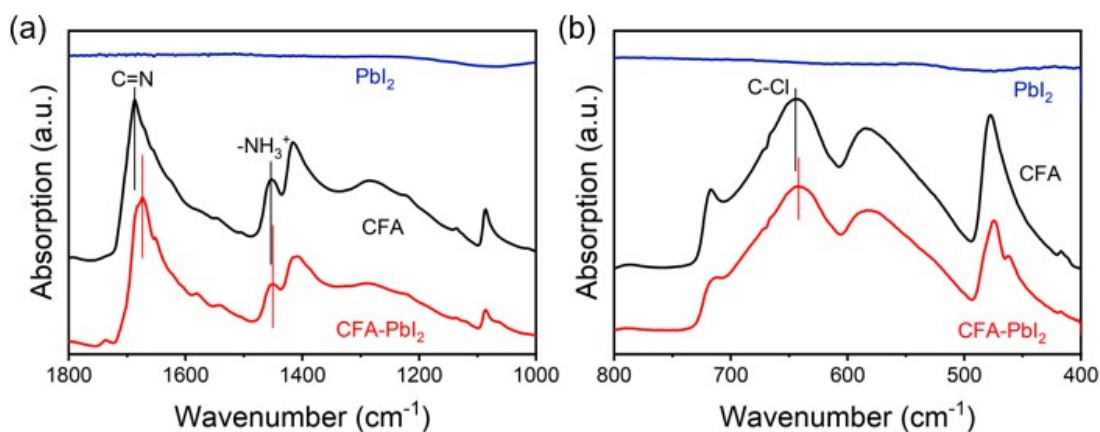


**Fig. S11.** ATR-FTIR spectra in the range of (a) 1800-1000 cm<sup>-1</sup> and (b) 800-400 cm<sup>-1</sup> of PbI<sub>2</sub>, CFA, CFA-PbI<sub>2</sub> samples.

The C=N stretching vibration peak of pristine CFA is at 1687 cm<sup>-1</sup>, which is reduced to 1674 cm<sup>-1</sup> in the CFA-PbI<sub>2</sub> sample.<sup>6</sup> The peak assigned to -NH<sub>3</sub><sup>+</sup> bend vibration appears at 1454 cm<sup>-1</sup> of pristine CFA, and is shifted toward decreased wavenumbers in the CFA-PbI<sub>2</sub> sample (1450 cm<sup>-1</sup>).<sup>6</sup> Moreover, the C-Cl stretching vibration peak at 645 cm<sup>-1</sup> of pristine CFA is reduced to 642 cm<sup>-1</sup> in the CFA-PbI<sub>2</sub> sample.<sup>7</sup> The peak shift demonstrates the chemical interaction between PbI<sub>2</sub> and CFA.

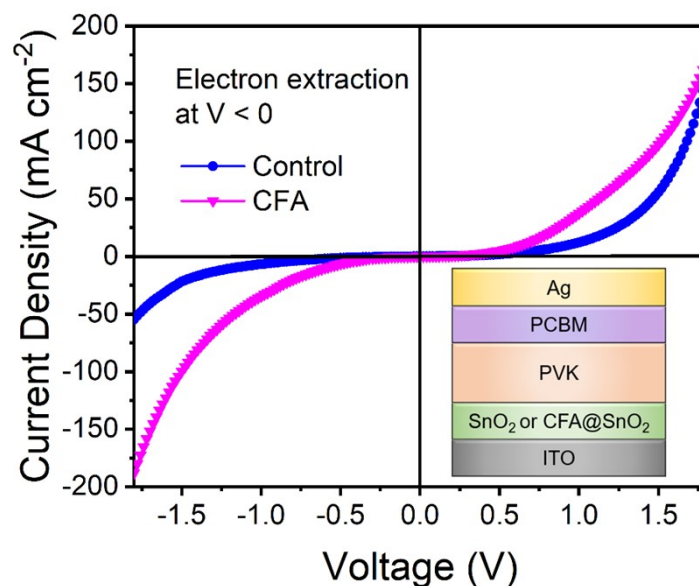


**Fig. S12.** J-V curves of electron-only devices under dark with SnO<sub>2</sub> and CFA@SnO<sub>2</sub> ETL, respectively. The inset displays the structure of the electron-only devices.

When a voltage is applied to the ITO electrode, electrons are injected to ETL from the perovskite layer. The J-V curve reveals that the CFA@SnO<sub>2</sub>-based device exhibits higher current density than the SnO<sub>2</sub>-based device at the same voltage, which indicates that the electron injection becomes easier from the perovskite layer to the CFA@SnO<sub>2</sub> ETL than to the SnO<sub>2</sub> ETL<sup>8</sup>.

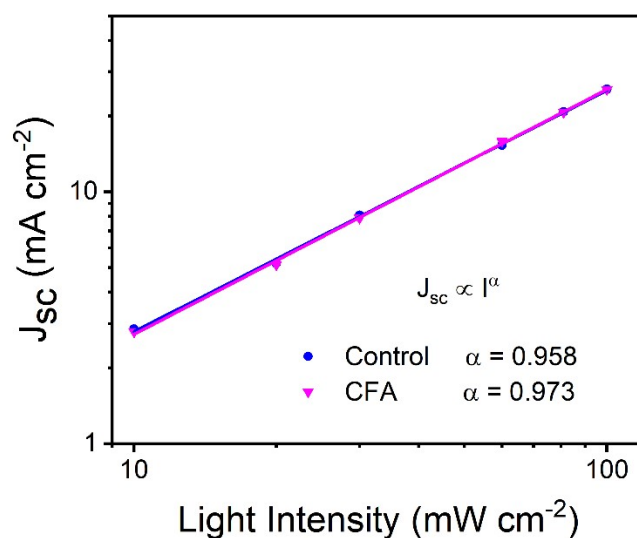


**Fig. S13.** J<sub>sc</sub> versus light intensity plots of PSCs based on SnO<sub>2</sub> and CFA@SnO<sub>2</sub> ETLS.

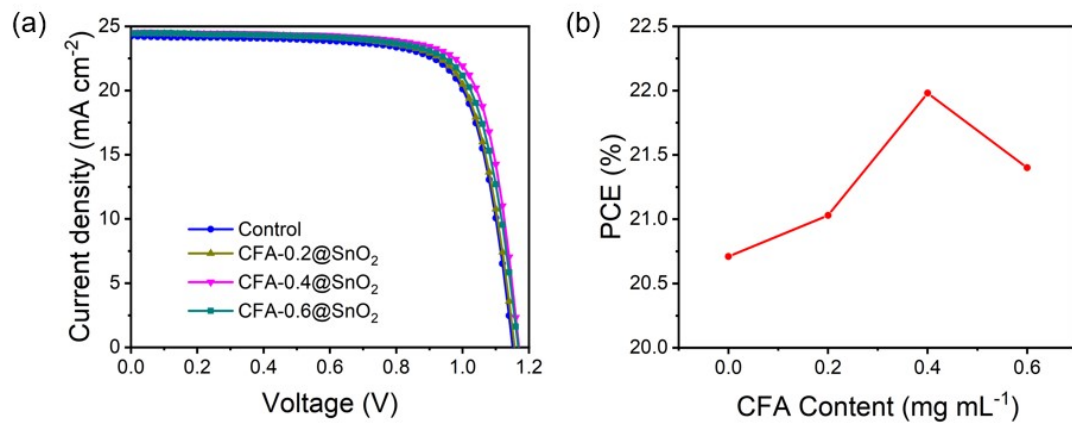


**Fig. S14.** (a) J-V curves and (b) PCE variation of PSCs with different amounts of CFA in SnO<sub>2</sub> ETLs. (0, 0.2, 0.4, 0.6 mg mL<sup>-1</sup>).

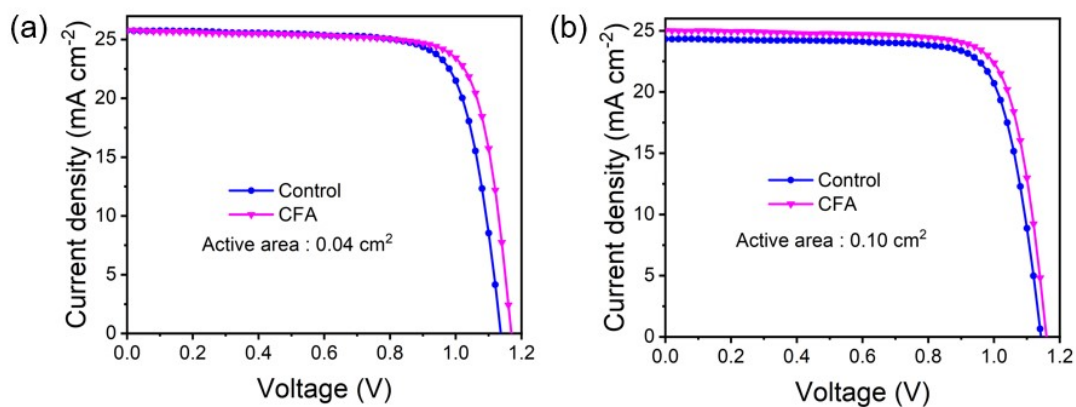


**Fig. S15.** J-V curves of champion devices based on SnO<sub>2</sub> and CFA@SnO<sub>2</sub> ETLs under reverse scan.

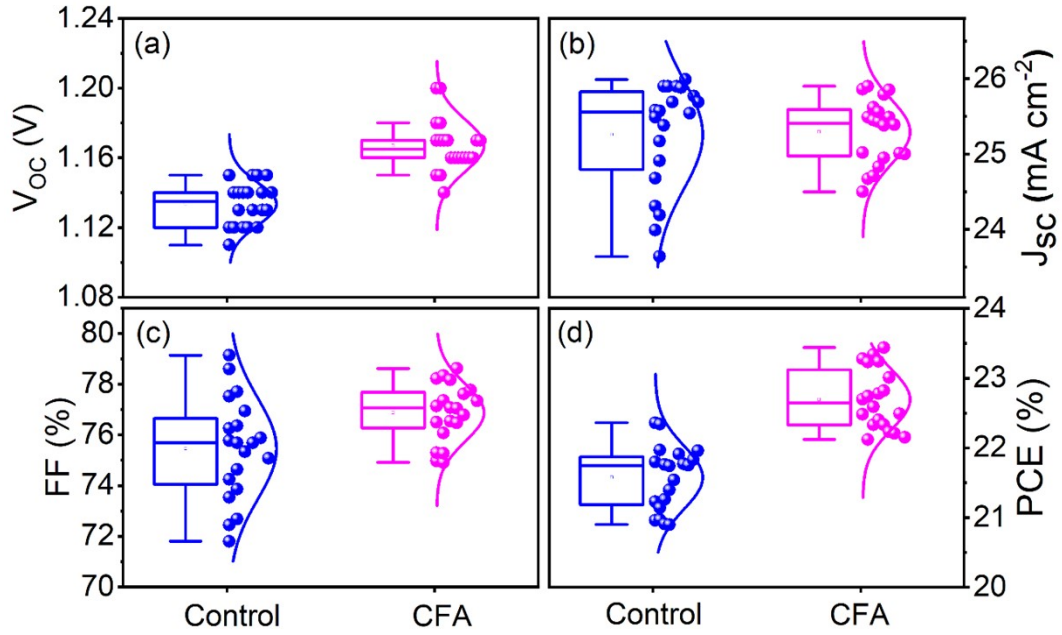


**Fig. S16.** Statistical distribution of the (a)  $V_{OC}$ , (b)  $J_{SC}$ , (c) FF and (d) PCE of  $SnO_2$ -based and CFA@ $SnO_2$ -based PSCs, respectively. The error bars were obtained from 20 measured samples for each condition (active area:  $0.04 \text{ cm}^2$ ).

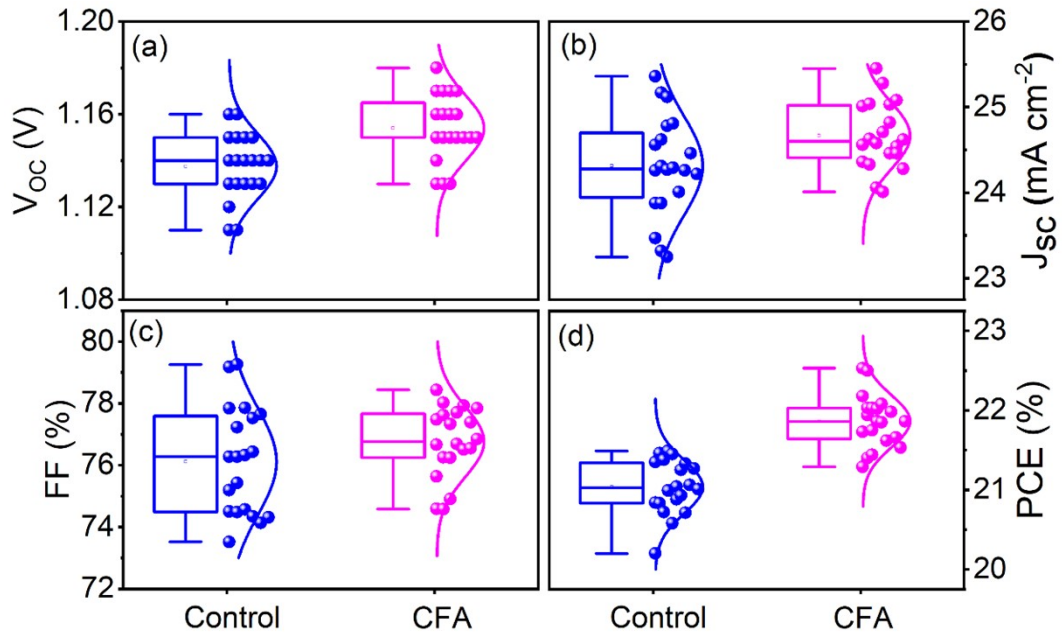


**Fig. S17.** Statistical distribution of the (a)  $V_{OC}$ , (b)  $J_{SC}$ , (c) FF and (d) PCE of  $SnO_2$ -based and CFA@ $SnO_2$ -based PSCs, respectively. The error bars were obtained from 20 measured samples for each condition (active area:  $0.10 \text{ cm}^2$ ).

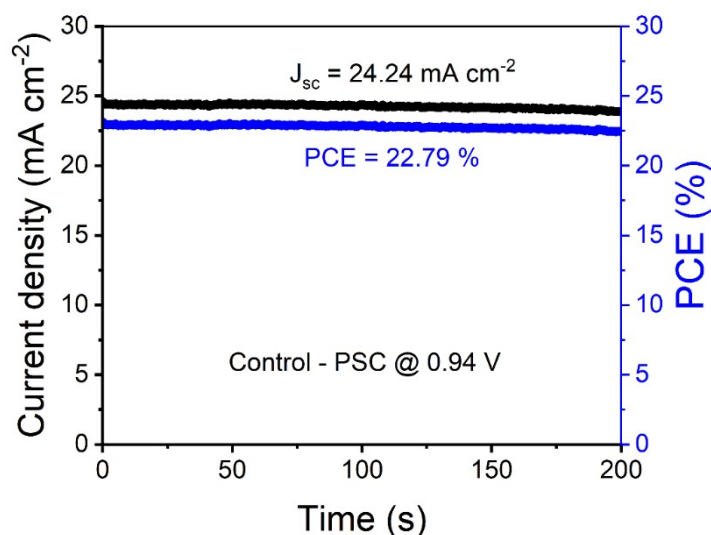


**Fig. S18.** Steady-state current density and PCE measured at a maximum power point of 0.94 V for the device based on SnO<sub>2</sub> ETL under AM 1.5G illumination (active area:0.04 cm<sup>2</sup>).

**Table S1.** Calculated relative amounts of lattice oxygen (O<sub>L</sub>) and vacancy oxygen (O<sub>V</sub>) for the SnO<sub>2</sub> and CFA@SnO<sub>2</sub> film by fitting peak area.

Films	O <sub>L</sub> (eV)	O <sub>L</sub> (%)	O <sub>V</sub> (eV)	O <sub>V</sub> (%)
SnO <sub>2</sub>	530.47	64.5	531.61	35.5
CFA@SnO <sub>2</sub>	530.44	72.5	531.66	27.5

**Table S2.** Calculated valence band maximum (E<sub>VBM</sub>) and conduction band minimum (E<sub>CBM</sub>) from E<sub>cut-off</sub>, E<sub>onset</sub> and E<sub>g</sub> for the SnO<sub>2</sub> and CFA@SnO<sub>2</sub> film.

Films	E <sub>cut-off</sub> (eV)	E <sub>F</sub> (eV)	E <sub>onset</sub> (eV)	E <sub>VBM</sub> (eV)	E <sub>g</sub> (eV)	E <sub>CBM</sub> (eV)
SnO <sub>2</sub>	16.26	-4.96	2.65	-7.61	4.24	-3.37
CFA@SnO <sub>2</sub>	16.41	-4.81	3.77	-8.58	4.25	-4.33

**Table S3.** Parameters of the TRPL spectra of perovskite films deposited on SnO<sub>2</sub> and CFA@SnO<sub>2</sub> substrates, respectively.

Films	τ <sub>1</sub> (ns)	A <sub>1</sub> (%)	τ <sub>2</sub> (ns)	A <sub>2</sub> (%)	τ <sub>ave</sub> (ns)
ITO / SnO <sub>2</sub> / PVK	134.83	16.55	590.31	83.45	570.57
ITO / CFA@SnO <sub>2</sub> / PVK	119.19	24.87	469.66	75.13	442.50

**Table S4.** Photovoltaic parameters of devices with different amounts of CFA in SnO<sub>2</sub> ETLs (active area: 0.1 cm<sup>2</sup>).

ETL	V <sub>OC</sub> (V)	J <sub>SC</sub> (mA cm <sup>-2</sup> )	FF (%)	PCE (%)
SnO <sub>2</sub>	1.15	24.22	74.31	20.70
CFA-0.2@SnO <sub>2</sub>	1.16	24.44	74.39	21.09
CFA-0.4@SnO <sub>2</sub>	1.17	24.54	76.55	21.98
CFA-0.6@SnO <sub>2</sub>	1.17	24.46	74.91	21.44

**Table S5.** Photovoltaic parameters of champion devices based on SnO<sub>2</sub> and CFA@SnO<sub>2</sub> ETL.

Active area (cm <sup>2</sup> )	Devices	V <sub>OC</sub> (V)	J <sub>SC</sub> (mA cm <sup>-2</sup> )	FF (%)	PCE (%)
0.04	Control	1.14	25.77	76.26	22.40 (21.57 ± 0.83) <sup>a</sup>
	CFA	1.17	25.79	77.77	23.47 (22.69 ± 0.78)
0.10	Control	1.14	24.31	77.23	21.40 (20.84 ± 0.56)
	CFA	1.16	25.01	77.71	22.54 (21.90 ± 0.64)

<sup>a</sup> The average PCE obtained from 20 devices and the standard error.

## References

- 1 Q. Jiang, Z. Chu, P. Wang, X. Yang, H. Liu, Y. Wang, Z. Yin, J. Wu, X. Zhang and J. You, *Adv. Mater.*, 2017, **29**, 1703852.
- 2 J. B. You, Y. M. Yang, Z. R. Hong, T. B. Song, L. Meng, Y. S. Liu, C. Y. Jiang, H. P. Zhou, W. H. Chang, G. Li and Y. Yang, *Appl. Phys. Lett.*, 2014, **105**, 183902.
- 3 P. N. Murgatroyd, *J. Phys. D: Appl. Phys.*, 1970, **3**, 151.
- 4 T. Bu, J. Li, F. Zheng, W. Chen, X. Wen, Z. Ku, Y. Peng, J. Zhong, Y. B. Cheng and F. Huang, *Nat. Commun.*, 2018, **9**, 4609.
- 5 Z. Liu, K. Deng, J. Hu and L. Li, *Angew. Chem., Int. Ed.*, 2019, **58**, 11497-11504.
- 6 X. Wang, Y. Fan, L. Wang, C. Chen, Z. Li, R. Liu, H. Meng, Z. Shao, X. Du, H. Zhang, G. Cui and S. Pang, *Chem*, 2020, **6**, 1369-1378.
- 7 D.-K. Kweon, N. Kawasaki, A. Nakayama and S. Aiba, *J. Appl. Polym. Sci.*, 2004, **92**, 1716-1723.
- 8 D. Yang, R. Yang, K. Wang, C. Wu, X. Zhu, J. Feng, X. Ren, G. Fang, S. Priya and S. F. Liu, *Nat. Commun.*, 2018, **9**, 3239.